Phylogeny, ultrastructure, and flagellar apparatus of a new marimonad flagellate *Abollifer globosa* sp. nov. (Imbricatea, Cercozoa)

Takashi Shiratori[a], Akiko Yokoyama[b], and Ken-Ichiro Ishida[b,1]

[a]Graduate School of Life and Environmental Sciences, University of Tsukuba, Tsukuba, Ibaraki 305-8572, Japan;

[b]Faculty of Life and Environmental Sciences, University of Tsukuba, Tsukuba, Ibaraki 305-8572, Japan

Running title: Description of *Abollifer globosa* sp. nov.

[1] Corresponding Author: FAX +81 298 53 4533

e-mail ken@biol.tsukuba.ac.jp (K. Ishida)

Abollifer is little-known genus of marine heterotrophic flagellates with no ultrastructural and molecular information, and its taxonomic position remains uncertain. In this study, we report a new species of *Abollifer*, *Abollifer globosa* sp. nov., isolated from a seawater sample collected at Tokyo Bay. To reveal the taxonomic position and morphological characteristics of *A. globosa*, we performed light and electron microscopic observations and a phylogenetic analysis using small subunit ribosomal DNA sequences. *A. globosa* cells were 29.5 μm in length and 22.4 μm in width, oval or ovoid in shape with an apical projection. Two unequal flagella emerged from a deep subapical flagellar pit. The rim of the flagellar pit except for the ventral side swelled. Electron microscopic observations showed that *A. globosa* possessed mitochondria with tubular cristae, Golgi apparatuses, microbodies, extrusomes, and many symbiotic bacteria. Basal bodies were arranged in parallel. The flagellar apparatus of *A. globosa* showed affinity with common gliding cercozoan flagellates. Our phylogenetic tree showed that *A. globosa* branched as the sister position of order Marimonadida (Imbricatea, Cercozoa). On the basis of morphological and molecular phylogenetic analysis, we conclude that *A. globosa* is a new member of the order Marimonadida.

Key words: Cercozoa; Marimonadida; heterotrophic flagellate; ultrastructure; phylogenetic analysis; flagellar apparatus.

Introduction

Imbricatea is one of the cercozoan classes that was established by Cavalier-Smith and Chao (2003) and originally included amoeboflagellates with many two-tiered siliceous scales (Thaumatomonadida) and filose amoebae covered by a siliceous shell (Euglyphida). Although the original Imbricatea had been a morphologically well-characterized group based on extracellular siliceous materials, recent phylogenetic analyses have shown that several non-silicated heterotrophic flagellates are closely related to the silica-depositing imbricateans (e.g., *Clautriavia*, *Nudifila*, *Pseudopirsonia*, and *Spongomonas*) (Bass and Cavalier-Smith 2004; Chantangsi and Leander 2010; Howe et al. 2011), and now Imbricatea includes various heterotrophic flagellates and amoebae with or without siliceous scales (Adl et al. 2012; Howe et al. 2011).

Order Marimonadida is a recently established group of Imbricatea (Howe et al. 2011). It consists of three genera and species of marine naked heterotrophic flagellates (*Auranticordis quadriverberis*, *Pseudopirsonia mucosa*, and *Rhabdamoeba marina*). *A. quadriverberis* is a large, orange-colored flagellate with four subapically inserted, posterior-directed flagella and many cyanobacterial endosymbionts (Chantangsi et al. 2008). *P. mucosa* is a small swimming biflagellate that is parasitic to diatoms (Kühn et al. 2004). Although the morphological affinity of *Auranticordis* and *Pseudopirsonia* is little known, the monophyly of these two genera is well supported by molecular phylogenetic analyses (e.g., Chantangsi et al. 2008; Howe et al. 2011; Yabuki and Ishida 2011). *R. marina* is a small amoeboflagellate that was previously regarded as a Protista incertae sedis (Rogerson et al. 1998). In Howe et al. (2011), *R. marina* is also included in Marimonadida on the basis of the similarity of flagellar arrangement with *A. quadriverberis*. However, there are no other shared characteristics between *R. marina* and *A. quadriverberis*, and the phylogenetic position of *Rhabdamoeba* is still unknown since no molecular data for this species has been

available. Considering that the three species that make up Marimonadida show very different morphology from each other, cryptic lineages that fill the morphological gaps among the marimonads may exist. In fact, there are several environmental sequences that branch within or near the clade of marimonads (Chantangsi et al. 2008; Howe et al. 2011). Thus, further taxonomic studies on the marimonads are necessary for understanding their hidden diversity.

Recently, we established a cultured strain of a heterotrophic flagellate (strain DA172) from a seawater sample collected in Tokyo Bay. Although the feeding behavior and the chlorophyll metabolism of the strain have been described in a previous study (Kashiyama et al. 2012), the taxonomic study on this flagellate has not been performed. On the basis of cell size, movement, and a unique flagellar pit rimmed by a collar-like structure, we temporarily identified the strain as a member of genus *Abollifer*. Since Vørs (1992) described this genus based on the type species *A. prolabens*, *Abollifer* has not been reported from any environmental samples and its taxonomic position remains uncertain. To elucidate the taxonomic position of strain DA172, we performed a molecular phylogenetic analysis using small subunit ribosomal DNA (SSU rDNA) sequences and electron microscopic observations. According to the SSU rDNA phylogeny, strain DA172 branched as the sister lineage of the marimonad clade, while our detailed ultrastructural observations showed affinities with other imbricatean flagellates. Unique ultrastructural characteristics that have not been reported from the marimonads were also observed. Based on the results of the molecular phylogenetic analysis and microscopic observations, we propose that strain DA172 is a new species of *Abollifer* and place it in Imbricatea. These findings provide helpful information for understanding ultrastructural evolution within Imbricatea.

Results

Light microscopy.

Cells were subglobose or ovoid with an apical projection, 29.5 (24.5–40.9) μm long and 22.4 (18.9–33.5) μm wide (n = 24) (Fig. 1A, B). Many small granules were observed on the surface of the cell (Fig. 1A, B). A large conspicuous nucleus was located in the anterior half of the cell (Fig. 1A). Cells contained many vacuoles and oil drops (Fig. 1A, B). Two unequal flagella emerged from a deep subapical flagellar pit (Fig. 1A–C). The rim of the flagellar pit except for the ventral side swelled and the ventral rim of the flagellar pit was continuous with the rim of a short ventral groove (Fig. 1B). The dorsal rim of the flagellar pit was occasionally protrusive like a rostrum. The short anterior flagellum was approximately 10.9 μm long (8.4–13.4 μm, n = 16) and the long posterior flagellum was approximately 35 μm long (32.4–37.5 μm, n = 14). Cells sometimes showed smooth gliding movement; the anterior flagellum waved and directed to the left side of the cell and the posterior flagellum was entirely attached to the substrate and directed to the posterior sides of the cell (Fig. 1C). Floating and sinking cells unattached to the substrate were also occasionally observed in culture flasks. Non-granular lobose pseudopodia were occasionally observed (Fig. 1D). Although cells seemed to be rigid, their shape could change dramatically when feeding on diatoms (Fig. 1E). The cells were reproduced by longitudinal binary division. Multinucleate cells with several flagellar sets were occasionally observed. Cysts were not observed.

Electron microscopy.

In scanning electron microscopy, many small pits were observed over the entire surface of the cell (Fig. 2). It was not clear whether these pits were vestiges of discharged extrusomes or fixation artifacts. Two naked flagella were emerged from a subapical flagellar pit (Fig. 2, 3). The rim of the flagellar pit except for the ventral side swelled, and the short ventral

groove was continuous with the opening of the flagellar pit (Fig. 2). The rim of the flagellar pit looks like the lapel of a coat (Fig. 2). The flagellar pit and the short ventral groove were circled with a shallow oval furrow that emerged from the dorsal rim of the flagellar pit (Fig. 3).

Transmission electron microscopic observations showed that cells were surrounded only by a plasma membrane (Fig. 4A), and globular extrusomes were located sparsely just beneath the plasma membrane (Fig. 4B). Cells possessed many vacuoles in the cytoplasm (Fig. 4A, C). Mitochondria with tubular cristae, symbiotic bacteria, and small microbodies were scattered in the cytoplasm (Fig. 4C). The cells possessed a nucleus with permanently condensed chromatin and conspicuous nucleolus (Fig. 4A, C). The nucleus was located in the anterior part of the cell near the basal bodies and the flagellar pit (Fig. 4D). Two dictyosomes of Golgi apparatus were located beside the flagellar pit and the nucleus (Fig. 4D). Vesicles that contain slightly electron-dense amorphous materials were observed at the anterior region of the cell (Fig. 4D).

Two basal bodies were arranged in parallel; the anterior flagellum located at the left side in the flagellar pit, and the posterior flagellum located at the right side in the flagellar pit (Fig. 5A–C). Both basal bodies look identical in structural characteristics; a cartwheel structure was observed in approximately the lower third of the basal body (Fig. 5D). A thick electron dense plate was located at the transitional region (Fig. 5D). An axosome was placed just above the dense plate, at the level of the plasma membrane (Fig. 5D). Two basal bodies were connected by two fibrillar bridges (Fig. 5A, B). The anterior fibrillar bridge (fb1) was a large fibrous structure that emerged from the anterior side of both basal bodies and consisted of electron-dense edges and a less dense middle portion (Fig. 5A, B). The less dense portion of the fb1 had a thin partition in the middle (Fig. 5A, B). The posterior fibrillar bridge (fb2) was an electron-dense fiber that emerged from the

posterior side of both basal bodies (Fig. 5A). The fb1 and fb2 attached to striated fiber 1 and 2 (sb1 and sb2), respectively. The sb1 emerged from the right side of the fb1 and lined the anterior side of the flagellar pit bottom region (Fig. 5B, C, E). The sb2 emerged from the middle of the fb2 (Fig. 5A). The sb2 was less dense than the sb1 and lined the nuclear side of the flagella pit bottom region (Fig. 5A–C, E). Large fibrous material (lfm) was located near the anterior to dorsal side of the basal bodies (Fig. 5, 6). Although the basal bodies and the lfm were usually present near the nucleus, the basal bodies distant from the nucleus and a highly elongated lfm locating between them were occasionally observed (Fig. 6C). Although the structural relationship among the lfm, the basal bodies, and the nucleus could not be shown clearly, the lfm looked connecting the basal bodies and nucleus. A large vesicle that was closely associated with the lfm was observed (Fig. 5D, E, 6). At the proximal side of the basal bodies, the vesicle was invaginated by the lfm and formed a folded structure (Fig. 5D, E 6A, B, D). At the anterior side of the lfm, the vesicle was flattened since it was sandwiched between the lfm and an anterior row of microtubules (rm) (Fig. 5A–C, 6 B, E). The rm consisted of numerous microtubules was associated with the flat cisterna and lined the anterior side of the flagellar pit (Fig. 5A–C, E, 6A, B, E). The rm reached the tip of the flagellar pit (Fig. 6A). A microtubular band was observed just beneath of the ventral surface (Fig. 7). Although the entire structure of the microtubular band could not be uncovered in the serial sections, it appears to circle the flagellar pit and ventral groove (Fig. 7).

Since the arrangement of microtubular roots in strain DA172 seemed to be homologous to those of other gliding cercozoan flagellates, we applied terms used in previous studies of cercozoan flagellar apparatuses (e.g., Cavalier-Smith and Karpov 2011; Karpov 2010). The posterior basal body had one microtubular root; the ventral posterior root of the posterior flagellum (vp1), which originated from the right side of the posterior

basal body and ran along the right side of the flagella pit (Fig. 5D, 8G, 9B, F, G, 10B, C). The vp1 consisted of two microtubules (Fig. 10B, C). The anterior basal body had three microtubular roots; a ventral posterior root of the anterior flagellum (vp2), dorsal anterior root (da), dorsal posterior root (dp2) and secondary microtubules (sm). The vp2 originated from the proximal region of the left side of the anterior basal body (Fig. 5D, 8C, 9B, E). The vp2 passed the proximal side of the two basal bodies and ran along the right side of the flagellar pit and the posterior side of the vp1 (Fig. 5D, 8C–H, 9B, F,G). Although the vp2 consisted of seven microtubules at its origin, the distal end of the vp2 had only three microtubules (Fig. 8C–H, 10A–C). The da originated from the left side of the anterior basal body (Fig. 8A, B, 9A–F, 10G–I). Since electron dense material is associated with the da, the number of microtubules was not clear. However, it seemed to consisted of one or two microtubules and ran along the anterior side of the flagellar pit in front of the anterior flagellum (9A–F, 10G–I). Consisted of six microtubules, the dp2 originated from the left side of the anterior basal body, just above the origin of the da and ran along the left side of the flagellar pit (Fig. 5D, 8A, B, 9C, D, 10G–I). The sm originated from the proximal region of the da (Fig. 8A, B, 9C, D, 10G, H). It consisted of over ten microtubules and ran toward the posterior and ventral side of the cell (Fig. 8A, B, 9C, D, 10G, H). The left anterior root (lr) originated from the space between the two basal bodies and ran along the anterior side of the flagellar pit (Fig. 8D, E, 9F, G). Judging only from longitudinal sections, the lr seemed to be consisted of three microtubules (Fig. 9F, G), though a good cross section of the lr could not be observed and the number of microtubules for the lr is still uncirtain.

Phylogenetic analysis.

We determined almost the complete length (1,711 bp) of the SSU rDNA sequence for *A. globosa* to estimate its phylogenetic position. No intron was found in the SSU rDNA

sequence. Our phylogenetic tree inferred from the SSU rDNAs of various cercozoans and including the environmental sequences showed that *A. globosa* formed a clade with two marimonads (*Auranticordis quadriverberis* and *Pseudopirsonia mucosa*) and two environmental sequences (AY620332 and AY620359) with a bootstrap percentage (BP) of 63% and a Bayesian posterior probability (BPP) of 1.00 (Fig. 12). This clade branched as sister to the euglyphids, but with weak support, and the phylogenetic position of this clade was uncertain.

Taxonomic Treatment

Phylum Cercozoa

Class Imbricatea

Order Marimonadida

Abollifer **Vørs 1992, emend. Shiratori et al. 2014 (ICZN)**

Emended description. Gliding, floating heterotrophic marine flagellates with one long trailing flagellum, and sometimes with another short trailing or beating flagellum. The flagella emerging from a deep subapical flagellar pit. The rim of the flagellar pit swollen like the lapel of a coat. The short ventral groove connecting to the flagellar pit. A row of microtubules lining the anterior side of the flagellar pit. Large fibrous material near the basal bodies. Cells naked but with a rigid surface. Basal bodies parallel. Simple globular extrusome just beneath the plasma membrane. Presence of Golgi apparatus and microbodies.

Type species. *Abollifer prolabens*.

Abollifer globosa sp. nov. Shiratori et al. 2014 (ICZN)

Description. Cells subglobose or ovoid with apical projection. 29.5 (24.5–40.9) μm in length and 22.4 (18.9–33.5) μm in width, with beating short anterior flagellum 10.9 (8.4–13.4) μm and long posterior gliding flagellum 35 (32.4–37.5) μm. Dorsoventrally not

flat. Short ventral groove continuous with the opening of the flagellar pit. Dorsal rim of the flagellar pit occasionally protrusive. Lobose pseudopodia sometimes emerging. Cells reproduced by longitudinal binary division.

Hapantotype. One microscope slide (TNS-AL-xxxx), deposited in the herbarium of the National Museum of Nature and Science (TNS), Tokyo.

Isotype. One EM block (TNS-AL-xxxx) in TNS. These cells are derived from the same sample as the holotype.

Iconotype. Figure 1

DNA sequence: Small subunit ribosomal DNA, xxxxx.

Type locality: Seawater at wharf of Tokyo Bay, Japan (latitude = 35.6180°N, longitude = 139.7729°E).

Collection date: July 10, 2011

Authentic culture: The strain, DA172, used for describing this species is deposited in and maintained in the National Institute for the Environmental Sciences, Tokyo, as NIES-xxxx.

Etymology: *Globosus* (round or spherical) refers to the cell shape of this organism.

Discussion

Abollifer globosa sp. nov. is a new species of *Abollifer*.

Genus *Abollifer* was described based on a type species, *A. prolabens*, which is a gliding flagellate with a rigid surface, long trailing flagellum, and deep subapical flagellar pit of which the side is swollen like the lapel of the coat (Vørs 1992). The results of light and scanning electron microscopic observations on *A. globosa* conform to the characteristic features of genus *Abollifer*. On the other hand, *A. globosa* is bigger than *A. prolabens* (8–12 × 10–20 μm) and not dorsoventrally flattened (Vørs 1992). *A. globosa* is also different from *A. prolabens* in maintaining two flagella during the cell cycle. Therefore, we considered *A. globosa* as a new species of *Abollifer*. Since no molecular information of *A. prolabens* has been reported, this study first demonstrated the phylogenetic position of the genus *Abollifer*.

Ultrastructural comparison between *A. globosa* and other Imbricatean flagellates.

Our phylogenetic analysis using SSU rDNA showed that *A. globosa* is included in Cercozoa and branched as a basal lineage of a clade of Marimonadida that is a small and poorly studied order of class Imbricatea. Here, we performed an ultrastructural comparison between *A. globosa* and other imbricatean flagellates to reveal the taxonomic position of *Abollifer* and the evolution of imbricateans.

Extrusomes are widely observed among cercozoans (e.g., cercomonads, thaumatomonads, cryomonads, and chlorarachnea) and vary in shape and structure (Hibberd and Norris 1984; Mikrjukov 1995; Mylnikov and Karpov 2004; Schnepf and Kühn 2000; Shiratori et al. 2012). *A. globosa* has globular extrusomes that lack complex structures and are located beneath the plasma membrane. The simple globular extrusomes similar to *A. globosa* are reported from a gliding imbricatean flagellate *Clautriavia biflagellata* and a marimonad flagellate *Auranticordis quadriverberis* (Chantangsi et al.

2008; Chantangsi and Leander 2010). The vacuolated cytoplasm like in *A. globosa* was also reported in *C. biflagellata* and *A. quadriverberis* (Chantangsi et al. 2008; Chantangsi and Leander 2010). These characters may be synapomorphies among Marimonadida and *Clautriavia,* since *C. biflagellata* often branched as the sister position of Marimonadida in several phylogenetic studies, although the statistical supports are weak (Chantangsi and Leander 2010; Howe et al. 2011). Vesicles with slightly electron-dense amorphous materials were observed at the anterior region of the cell. Although their precise function is not known, the vesicles may play an important role for the cell since they were seen in the specific region of all cells. No homologous vesicle has been reported in other cercozoans, but a careful survey on the presence and absence of this vesicle in cercozoans including members of which ultrastructures have been reported is required.

The complete flagellar apparatuses of imbricatean species have been studied in thaumatomonads and spongomonads (Hibberd 1976; Karpov 2010/1; Strüder-Kypke and Hausmann 1998). Thaumatomonads and spongomonads often formed a clade in several phylogenetic analyses although the statistical supports were low (Bass and Cavalier-Smith 2004; Howe et al. 2011). Their basal bodies share characteristics such as parallel basal bodies and the presence of a dense plate above the transitional region. These characteristics were considered to be synapomorphies among the two groups or imbricatean flagellates (Howe et al. 2011), although several exceptions exist (Shiratori et al. 2012). *A. globosa*, which is a distinctive lineage from the thaumatomonads/spongomonads clade, has parallel basal bodies without dense plates. This may suggest that parallel basal bodies are a synapomorphy among imbricateans, and the dense plate may be acquired in the common ancestor of spongomonads and thaumatomonads after *A. globosa* branched.

A. globosa has complex and unique fibrous materials around the basal bodies. The most notable character is the lfm. It is a large fibrous structure and presents near the nucleus and basal bodies. The lfm has not been reported in Cercozoa. However, a striated fiber (rhizoplast) that locates between the basal body and nucleus was observed in several groups of cercozoan flagellates including thaumatomonads and spongomonads (Hess and Melkonian 2014; Hibberd 1976; Karpov 2010/1; Karpov et al. 2006). Although the lfm is clearly different from the rhizoplast in its largeness and lacking striated pattern, it possibly connects to the nucleus and the basal body like the rhizoplast. *A. globosa* has two striated fibers (sb1 and sb2) that originated from the fibrillar bridges and line the flagellar pit. These fibers are unusual in Cercozoa but only spongomonads have a striated fiber that lines the flagellar pit (Hibberd 1976). However, the striated fiber of spongomonads is smaller than that of *A. globosa* and originates from dorsal flagellum (Hibberd 1976). Therefore we don't know whether the striated fiber of spongomonads is identical with that of *A. globosa* or not.

The microtubular roots of *A. globosa* are similar to those of other gliding cercozoan flagellates in possessing vp1, vp2, da, and lr. The vp2 of *A. globosa* pass around the proximal end of the posterior basal body, line the flagellar pit, and along the posterior flagellum together with the vp1. The similar direction of vp roots has been reported in *Thaumatomonas* (Karpov 2010/1). *A. globosa* and *Thaumatomonas* also share the da with many secondary microtubules (Karpov 2010/1). On the other hand, the dp2 was only reported in *Eocercomonas ramosa*, which is distantly related to *A. globosa* (Karpov et al. 2006). These dp2 emerge from the right side of the anterior basal body, distal to the da, but that of *E. ramosa* run toward the cell posterior along the dorsal side.

The anterior side of the flagellar pit in *A. globosa* is supported by a row of numerous microtubules, and is not associated with the basal bodies. This microtubular band

is a unique structure that has never been reported in Cercozoa. Since these characteristics are never or rarely reported in Cercozoa, it is difficult to evaluate them from an evolutionary or taxonomic perspective. *A. globosa* also has another circular microtubular band that is not associated with the basal bodies. This microtubular band encircles the flagellar pit and ventral groove and seems to line the shallow oval furrow observed in SEM micrographs (Fig. 3; arrowheads). A ring shaped microtubules that encircle the rim of the flagellar pit was observed in spongomonads (Hibberd 1976; Strüder-Kypke and Hausmann 1998). It suggests that the microtubular ring may be acquired in the common ancestor of marimonad and spongomonad.

While our phylogenetic analysis showed the monophyly of *A. globosa* and marimonads with moderate statistical support, strong ultrastructural affinity between *A. globosa* and Marimonadida was not observed. The weak morphological affinity between *A. globosa* and other marimonads may be caused by insufficient ultrastructural data on marimonads. In this study, mainly based on the phylogenetic analysis, we concluded that *A. globosa*, and therefore genus *Abollifer*, is a new member of order Marimonadida. Basal body arrangement and fibrous and microtubular structures of *A. globosa* show some affinities with that of thaumatomonads and spongomonads. These shared characteristics are possibly synapomorphy of Imbricatea and its subgroups respectively. However, imbricatean flagellates without information of flagellar apparatus still exists (e.g. *Clautrivia* and *Nudifila*). Further ultrastructural studies including reconstruction of flagellar apparatus on them will help to understand evolution of Imbricatea.

Methods

Culture establishment: Cells of *Abollifer globosa* sp. nov. were observed in seawater samples at a wharf in Tokyo Bay, Japan from the end of June to the beginning of August, and most abundantly at the end of July, in 2011. In natural samples, cells prey on various centric diatoms (e.g., *Skeletonema*, *Thalassiosira*, and *Cyclotella*). A culture of *A. globosa* (strain DA172) was established using a single-cell isolation technique as follows; seawater from 1 m depth was collected with a Van Dorn water sampler (RIGO, Co. Ltd., Tokyo, Japan) at a wharf in Tokyo Bay, Japan (latitude = 35.6180°N, longitude = 139.7729°E) on July 10, 2011. Single cells of *A. globosa* were isolated from the sample and incubated with Daigo IMK medium (Nihon Pharmaceutical Co. Ltd., Tokyo, Japan) and *Skeletonema costatum* (strain DA123) that was pre-cultured from the same sample as prey. Isolated cells of *A. globosa* could not be cultivated with other algal strains (e.g., *Heterosigma akashiwo*, *Prorocentrum minimum*, and *Pyramimonas* sp.) that were also pre-cultured from the same collection site. The culture of *A. globosa* was kept at 18°C under a 14-h light/10-h dark cycle.

Light microscopy: Cultivated cells were placed into a glass bottom dish and observed using an Olympus IX71 inverted microscope (Olympus, Tokyo, Japan) equipped with an Olympus DP71 CCD camera (Olympus).

Electron microscopy: For scanning electron microscopy (SEM), a specimen was prepared as described in Yabuki and Ishida (2011). The specimen was sputter-coated with platinum-palladium using a Hitachi E-102 sputter-coating unit (Hitachi High-Technologies Corp., Tokyo, Japan) and observed using a JSM-6360F field emission SEM (JEOL, Tokyo, Japan).

A specimen for transmission electron microscopy (TEM) observation was prepared as follows; cultivated cells were centrifuged and fixed with pre-fixation for 1 h at room

temperature with a mixture of 2% (v/v) glutaraldehyde, 0.1 M sucrose, and 0.1 M sodium cacodylate buffer (pH 7.2, SCB). Fixed cells were washed with 0.2 M SCB three times. Cells were post-fixed with 1% (v/v) OsO_4 with 0.1 M SCB for 1 h at 4°C. Cells were washed with 0.2 M SCB two times. Dehydration was performed using a graded series of 30–100% ethanol (v/v). After dehydration, cells were placed in a 1:1 mixture of 100% ethanol and acetone for 10 min and acetone for 10 min for two cycles. Resin replacement was performed by a 1:1 mixture of acetone and Agar Low Viscosity Resin R1078 (Agar Scientific Ltd, Stansted, England) for 30 min and resin for 2 h. Resin was polymerized by heating at 60°C for 8 h. Ultrathin sections were prepared on a Reichert Ultracut S ultramicrotome (Leica, Vienna, Austria), double stained with 2% (w/v) uranyl acetate and lead citrate (Hanaichi et al. 1986; Sato 1968), and observed using a Hitachi H-7650 electron microscope (Hitachi High-Technologies Corp., Tokyo, Japan) equipped with a Veleta TEM CCD camera (Olympus Soft Imaging System, Munster, Germany).

DNA extraction and polymerase chain reaction (PCR): Cells in the culture were centrifuged and total DNA was extracted from the pellet using a DNeasy Plant mini kit (Qiagen Science, Valencia, CA), according to the manufacturer's instructions. SSU rRNA of strain DA172 was amplified by polymerase chain reaction (PCR) with 18F-18R primers (Yabuki et al. 2010). Amplifications consisted of 30 cycles of denaturation at 94°C for 30 s, annealing at 55°C for 30 sec, and extension at 72°C for 2 min. An additional extension for 4 min at 72°C was performed at the end of the reaction. Amplified DNA fragments were purified after gel electrophoreses with a QIAquick Gel Extraction Kit (Qiagen Science), and then cloned into the pGEM® T-easy vector (Promega, Tokyo, Japan). The insert DNA fragments were completely sequenced by a 3130 Genetic Analyzer (Applied Biosystems, Monza, Italy) with a BigDye Terminator v3.1 cycle sequencing kit (Applied Biosystems, Monza, Italy). The SSU rDNA sequences of strain DA172 were deposited as xxxx,

respectively, in GenBank.

Sequence alignments and phylogenetic analysis: The SSU rDNA sequence of strain DA172 was added to our SSU rDNA alignment set of cercozoans. The sequences of the alignment set were automatically aligned with MAFFT (Katoh and Toh 2008) and then edited manually with SeaView (Galtier et al. 1996). For phylogenetic analyses, ambiguously aligned regions were manually deleted from each alignment. Finally, we prepared SSU rDNA alignments (1,641 positions). The alignment files that were used in the analyses are available on request. The maximum likelihood (ML) tree was heuristically searched using RAxML v.7.2.6 (Stamatakis 2006) under the GTR+Γ model. Tree searches started with 20 randomized maximum-parsimony trees, and the highest log likelihood (lnL) was selected as the ML tree. An ML bootstrap analysis (1000 replicates) was conducted under the GTR+Γ model with rapid bootstrap option. A Bayesian analysis was run using MrBayes v. 3.1.2 (Ronquist and Huelsenbeck 2003) with the GTR +Γ model for each dataset. One cold and three heated Markov chain Monte Carlo simulations with default chain temperatures were run for 7×10^6 generations, sampling lnL values and trees at 100-generation intervals. The first 2×10^6 generations of each analysis were discarded as "burn-in." Bayesian posterior probability (BPP) and branch lengths were calculated from the remaining trees.

Acknowledgements

This work was supported by JSPS KAKENHI Grant Numbers 13J00587 and 21247010.

References

Adl SM, Simpson AGB, Lane CE, Lukeš J, Bass D, Bowser SS, Brown MW, Burki F, Dunthorn M, Hampl V, Heiss A, Hoppenrath M, Lara E, Le Gall L, Lynn DH, McManus H, Mitchell EAD, Mozley-Stanridge SE, Parfrey LW, Pawlowski J, Rueckert S, Shadwick L, Schoch CL, Smirnov A, Spiegel FW (2012) The revised classification of eukaryotes. J Eukaryot Microbiol **59**:429–493

Bass D, Cavalier-Smith T (2004) Phylum-specific environmental DNA analysis reveals remarkably high global biodiversity of Cercozoa (Protozoa). Int J Syst Evol Microbiol **54**:2393–2404

Cavalier-Smith T, Chao EE (2003) Phylogeny and classification of phylum Cercozoa (Protozoa). Protist 154:341–358

Cavalier-Smith T, Karpov SA (2011) *Paracercomonas* kinetid ultrastructure, origins of the body plan of Cercomonadida, and cytoskeleton evolution in Cercozoa. Protist **163**:47–75

Chantangsi C, Esson HJ, Leander BS (2008) Morphology and molecular phylogeny of a marine interstitial tetraflagellate with putative endosymbionts: *Auranticordis quadriverberis* n. gen. et sp. (Cercozoa). BMC Microbiol **8**:123

Cavalier-Smith T, Oates B (2011) Ultrastructure of *Allapsa vibrans* and the Body Plan of Glissomonadida (Cercozoa). Protist **163**:165–187

Chantangsi C, Leander BS (2010) Ultrastructure, life cycle and molecular phylogenetic position of a novel marine sand-dwelling cercozoan: *Clautriavia biflagellata* sp. nov. Protist 161:133–147

Galtier N, Gouy M (1996) SEAVIEW and PHYLO_WIN: two graphic tools for sequence alignment and molecular phylogeny. Comput Appl Biosci **12**:543–548

Hanaichi T, Sato T, Hoshino M, Mizuno N (1986) A stable lead stain by modification of Sato's method. Proceedings of the XIth International Congress on Electron Microscopy, Japanese Society for Electron Microscopy, Kyoto, Japan, pp. 2181–2182

Hess S, Melkonian M (2014) Ultrastructure of the Algivorous Amoeboflagellate *Viridiraptor invadens* (Glissomonadida, Cercozoa). Protist **165**:605–635

Hibberd DJ (1976) The fine structure of the colonial colorless flagellates *Rhipidodendron splendidum* Stein and *Spongomonas uvella* Stein with special reference to the flagellar apparatus. J Protozool **23**:374–385

Hibberd DJ, Norris RE (1984) Cytology and ultrastructure of *Chlorarachnion reptans* (Chlorarachniophyta divisio nova, Chlorarachniophyceae classis nova). J Phycol **20**:310–330

Howe A, Bass D, Scoble J, Lewis R, Vickerman K, Arndt H, Cavalier-Smith T (2011) Novel cultured protists identify deep-branching environmental DNA clades of Cercozoa: new genera *Tremula*, *Micrometopion*, *Minimassisteria*, *Nudifila*, *Peregrinia*. Protist **162**:332–372

Karpov SA (2010/1) Flagellar apparatus structure of *Thaumatomonas* (Thaumatomonadida) and thaumatomonad relationships. Protistology **6**:326–344

Karpov SA, Bass D, Mylnikov AP, Cavalier-Smith T (2006) Molecular phylogeny of Cercomonadidae and kinetid patterns of *Cercomonas* and *Eocercomonas* gen. nov. (Cercomonadida, Cercozoa). Protist **157**:125–158

Kashiyama Y, Yokoyama A, Kinoshita Y, Shoji S, Miyashiya H, Shiratori T, Suga H, Ishikawa K, Ishikawa Akira, Inouye I, Ishida K, Fujinuma D, Aoki K, Kobayashi M, Nomoto S, Mizoguchi T, Tamiaki H (2012) Ubiquity and quantitative significance of detoxification catabolism of chlorophyll associated with protistan herbivory. Proc Natl Acad Sci USA **109**:17328–17335

Katoh K, Toh H (2008) Recent developments in the MAFFT multiple sequence alignment program. Brief Bioinform **9**:286–298

Kühn S, Medlin L, Eller G (2004) Phylogenetic position of the parasitoid nanoflagellate *Pirsonia* inferred from nuclear- encoded small subunit ribosomal DNA and a description of *Pseudopirsonia* n. gen. and *Pseudopirsonia mucosa* (Drebes) comb. nov. Protist **155**:143–156

Mikrjukov K (1995) Structure, function, and formation of extrusive organelles-microtoxicysts in the rhizopod *Penardia cometa*. Protoplasma **188**:186–191

Mylnikov AP, Karpov SA (2004) Review of the diversity and taxonomy of cercomonads. Protistology 3:201–217

Rogerson A, Hannah FJ, Anderson OR (1998) A redescription of *Rhabdamoeba marina*, an inconspicuous marine amoeba from benthic sediments. Invert Biol **117**:261–270

Ronquist F, Huelsenbeck JP (2003) MRBAYES 3: Bayesian phylogenetic inference under mixed models. Bioinformatics **19**:1572–1574

Sato T (1968) A modified method for lead staining of thin sections. J Electron Microsc **17**:158–159

Schnepf E, Kühn SF (2000) Food uptake and fine structure of *Cryothecomonas longipes* sp. nov., a marine nanoflagellate incertae sedis feeding phagotrophically on large diatoms. Helgol Mar Res **54**:18–32

Shiratori T, Yabuki, A, Ishida K (2012) *Esquamula lacrimiformis* n. g., n. sp., a new member of thaumatomonads that lacks siliceous scales. J Eukaryot Microbiol (in press)

Stamatakis A (2006) RAxML-VI-HPC: maximum likelihood-based phylogenetic analyses with thousands of taxa and mixed models. Bioinformatics **22**:2688–2690

Strüder-Kypke MC, Hausmann K (1998) Ultrastructure of the heterotrophic flagellates *Cyathobodo* sp., *Rhipidodendron huxleyi* Kent, 1880, *Spongomonas saccculus* Kent, 1880, and *Spongomonas* sp. Eur J Protistol **34**:376–390

Vørs N (1992) Heterotrophic amoebae, flagellates and Heliozoa from the Tvarminne area, Gulf of Finland, in 1988-1990. Ophelia **36**:1–109

Yabuki A, Inagaki Y, Ishida K (2010) *Palpitomonas bilix* gen. et sp. nov.: a novel deep-branching heterotroph possibly related to Archaeplastida or Hacrobia. Protist **161**:523–538

Yabuki A, Ishida K (2011) *Mataza hastifera* n. g., n. sp.: a possible new lineage in the Thecofilosea (Cercozoa). J Eukaryot Microbiol **58**:94–102

Figure 1. Differential interference contrast (DIC) micrographs of *Abollifer globosa* sp. nov. fp, flagellar pit; N, nucleus; oi, oil drop; p, pseudopodium; vg, short ventral groove. White arrows indicate flagellum; white arrowheads indicate small granule on the surface of the cell; white double arrowheads indicate large vacuoles. **A–C.** Gliding cells. **D.** Cell with lobose pseudopodium. **E.** Elongated cell digesting a diatom (*Skeletonema*). Scale bar: 10 µm.

Figure 2. Scanning electron micrograph of *Abollifer globosa* sp. nov. vg, short ventral groove. Scale bar: 10 µm.

Figure 3. High magnification scanning electron micrograph of the flagellar pit of *Abollifer globosa* sp. nov. Quadruple arrowheads indicate shallow oval furrow surrounding the flagellar pit and ventral groove. Scale bar = 5 µm.

Figure 4. Transmission electron micrographs of *Abollifer globosa* sp. nov. B, symbiotic bacteria; fp, flagellar pit; g, Golgi apparatus; mt, mitochondrion; mb, microbody; N, nucleus; n, nucleolus; double arrowheads indicate extrusome. Triple arrowheads indicate vesicles with ribbon-shaped materials. **A.** General cell image of *A. globosa*. Scale bar = 5 µm. **B.** High magnification view of the surface of the cell. Scale bar = 1 µm. **C** Cross-section of the anterior region of the cell. Scale bar = 1 µm. **D.** Highly vacuolated cytoplasm. Scale bar = 2 µm.

Figure 5. High magnification transmission electron micrographs of basal bodies of *Abollifer globosa* sp. nov. ab, anterior basal body; af, anterior flagellum; ax, axosome; d, dense transitional plate; dp2, dorsal posterior root from anterior flagellum; fb1, anterior

fibrillar bridge; fb2, posterior fibrillar bridge; lfm, large fibrous material N, nucleus; pb, posterior basal body; pf, posterior flagellum; sb1, anterior striated fiber; sb2, posterior striated fiber; vp1, ventral posterior root of posterior flagellum; vp2, ventral posterior root of anterior flagellum. Arrows indicate row of microtubules (rm). Arrowheads indicate flat cisterna attached to the anterior side of the lfm. Asterisks indicate vesicle that invaginates to the lfm. **A–C;** Selected consecutive cross-sections of two basal bodies (viewed from base to tip of basal bodies). Scale bar = 1 μm. **A.** A cross-section just above the cartwheel structures of two basal bodies. **B.** A cross-section through the proximal level of the plasma membrane. **C.** A cross-section of two flagella. **D.** Longitudinal section of two basal bodies. Scale bar = 500 nm. **E.** Longitudinal section of posterior basal body. Scale bar = 500 nm.

Figure 6. Transmission electron micrographs of *Abollifer globosa* sp. nov. b, basal body; lfm, large fibrous material; mt, mitochondrion; mb, microbody; N, nucleus. Arrows indicate anterior row of microtubules (rm). Arrowheads indicate flat cisterna attached to the anterior side of the lfm. Asterisks indicate vesicle that invaginates to the lfm. **A.** Longitudinal section of flagellar pit. Scale bar = 1 μm. **B.** High magnification view of longitudinal section of lfm. Scale bar = 1 μm. **C.** Elongated lfm connected to the anterior side of the nucleus. Scale bar = 1 μm. **D.** A cross-section of lfm. Scale bar = 2 μm. **E.** A cross-section of lfm through the proximal level of the basal body. Scale bar = 500 nm.

Figure 7. Transmission electron micrographs of *Abollifer globosa* sp. nov. ab, anterior basal body; fp, flagellar pit; lfm, large fibrous material; mt, mitochondrion; N, nucleus; vg, ventral groove. Arrows indicate anterior row of microtubules (rm). Double arrows indicate circular microtubule band. **A.** Longitudinal section of flagellar pit. Scale bar = 2 μm. **B.** High magnification view of fig. 6A, showing transverse section of the circular microtubule

band. Scale bar = 500 nm. **C.** Anterior region of the cell, showing the circular microtubule band runs transversally. Scale bar = 1 μm **D.** Transverse section of the distal end of the flagellar pit. Scale bar = 2 μm. **E.** High magnification view of fig. 6D, showing the circular microtubule band. Scale bar = 1μm. **F.** Longitudinal section? of the circular microtubule band. Scale bar = 2 μm. **G.** High magnification view of fig. 6F, showing the circular microtubule band. Scale bar = 1 μm.

Figure 8. Selected consecutive sections of two basal bodies of *Abollifer globosa* sp. nov. ab, anterior basal body; af, anterior flagellum; da, dorsal anterior root; dp2, dorsal posterior root from anterior flagellum; lfm, large fibrous material; lr, left anterior root; pf, posterior flagellum; sb1, anterior fibrillar bridge; sm, secondarily microtubules; vp1, ventral posterior root of posterior flagellum; vp2, ventral posterior root of anterior flagellum. Arrows indicate anterior row of microtubules (rm). Arrowheads indicate flat cisterna attached to the anterior side of the lfm. Triple arrowheads indicate vesicles with ribbon-shaped materials. Asterisks indicate vesicle that invaginates to the lfm. Scale bar = 500 nm. **A-H.** Approximately longitudinal section of two basal bodies (viewed from left side of the cell).

Figure 9. Selected consecutive sections of two basal bodies of *Abollifer globosa* sp. nov. ab, anterior basal body; da, dorsal anterior root; dp2, dorsal posterior root from anterior flagellum; fb1, anterior fibrillar bridge; fb2, posterior fibrillar bridge; lfm, large fibrous material; lr, left anterior root; pb, posterior basal body; pf, posterior flagellum; sb1, anterior fibrillar bridge; sm, secondarily microtubules; vp1, ventral posterior root of posterior flagellum; vp2, ventral posterior root of anterior flagellum. Arrows indicate anterior row of microtubules (rm). Asterisks indicate vesicle that invaginates to the lfm. Scale bars = 500

nm. **A–D.** Approximately longitudinal sections of two basal bodies (viewed from posteriorside of the cell). **E–G.** Approximately longitudinal sections of posterior basal bodies (viewed from left posterior side of the cell).

Figure 10. Selected consecutive sections of two basal bodies of *Abollifer globosa* sp. nov. ab, anterior basal body (viewed from ventral side of the cell). af, anterior flagellum; da, dorsal anterior root; dp2, dorsal posterior root from anterior flagellum; pb, posterior basal body; sm, secondarily microtubules; vp1, ventral posterior root of posterior flagellum; vp2, ventral posterior root of anterior flagellum. Scale bar = 500 nm. **A-F.** High magnification view of the transverse section of the posterior basal body. **G-I.** High magnification view of the transverse section of the anterior basal body.

Figure 11. Illustration of the microtubules and fibrous structures of *Abollifer globosa* sp. nov. ab, anterior basal body; af, anterior flagellum; da, dorsal anterior root; dp2, dorsal posterior root from anterior flagellum; fb1, anterior fibrillar bridge; fb2, posterior fibrillar bridge; lfm, large fibrous material lr, left anterior root; N, nucleus; pb, posterior basal body; pf, posterior flagellum; sb1, anterior fibrillar bridge; sm, secondarily microtubules; vp1, ventral posterior root of posterior flagellum; vp2, ventral posterior root of anterior flagellum. Asterisk indicates a large vesicle that closely associates with lfm. **A**. Left lateral view of the cell. **B**. Detailed structures around basal body and flagellar pit. **C.** Detailed structure of microtubular roots.

Figure 12. Maximum-likelihood tree of 89 cercozoans using 1,641 positions of the small subunit ribosomal DNA (SSU rDNA). Environmental sequences were labeled with accession numbers. Only bootstrap support ≥ 50% is shown. Nodes supported by Bayesian

posterior probabilities ≥ 0.95 are highlighted by bold lines.

Fig. 1

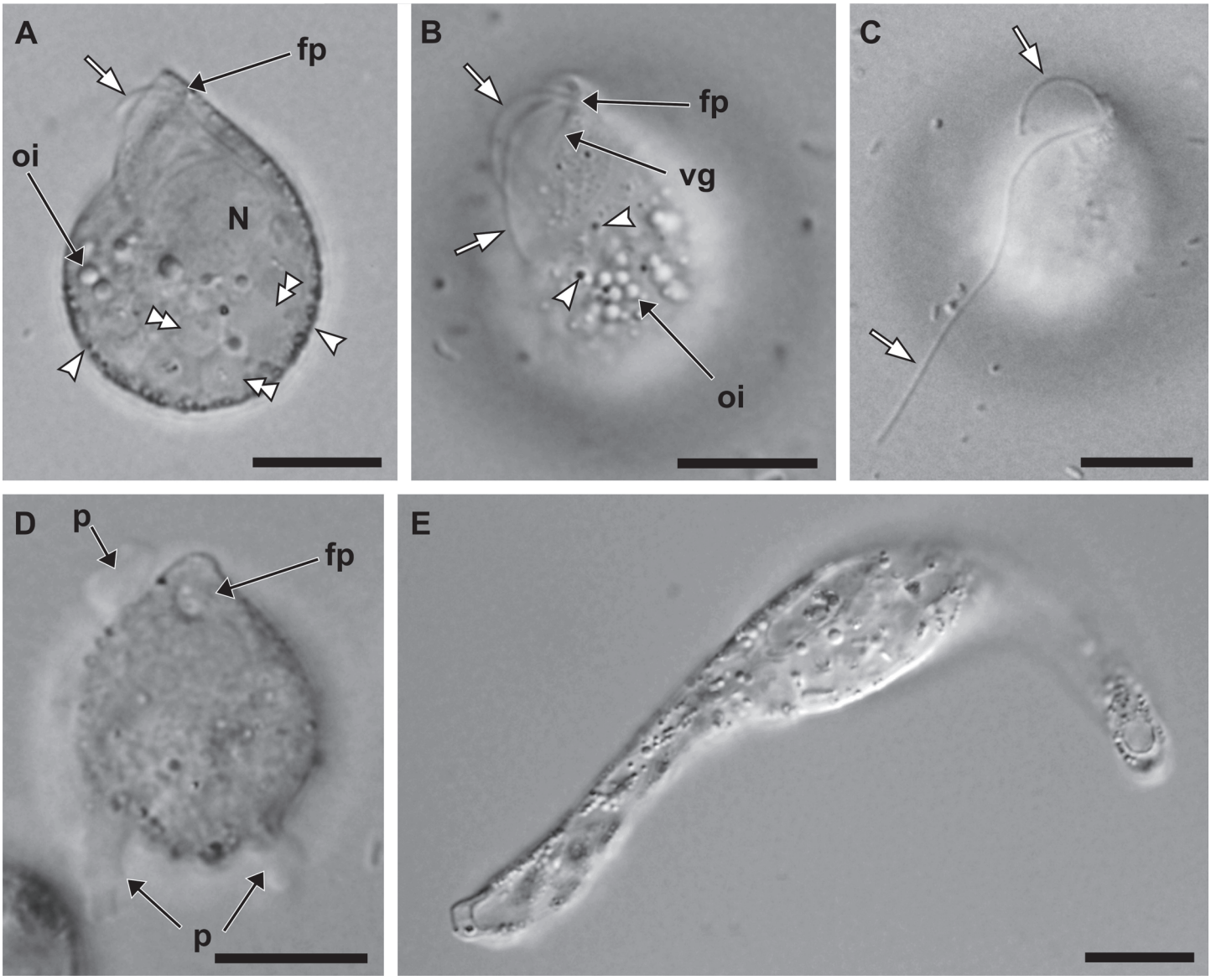

Fig. 2

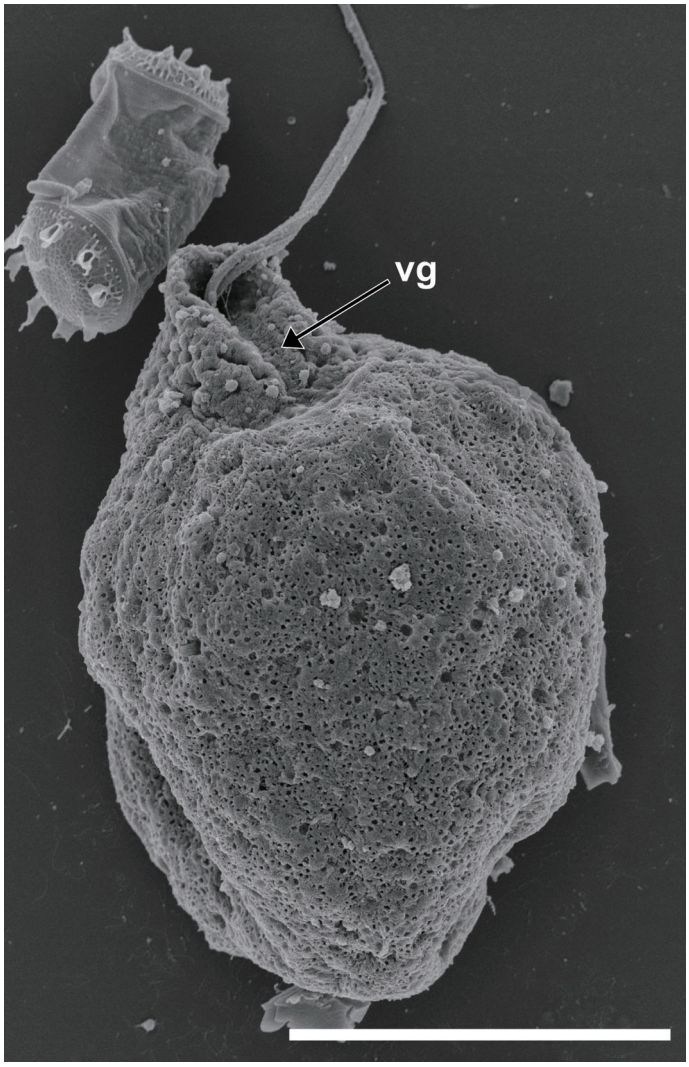

Fig. 3

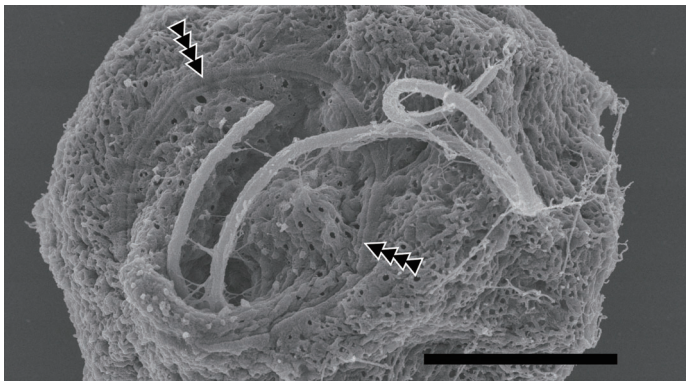

Fig. 4

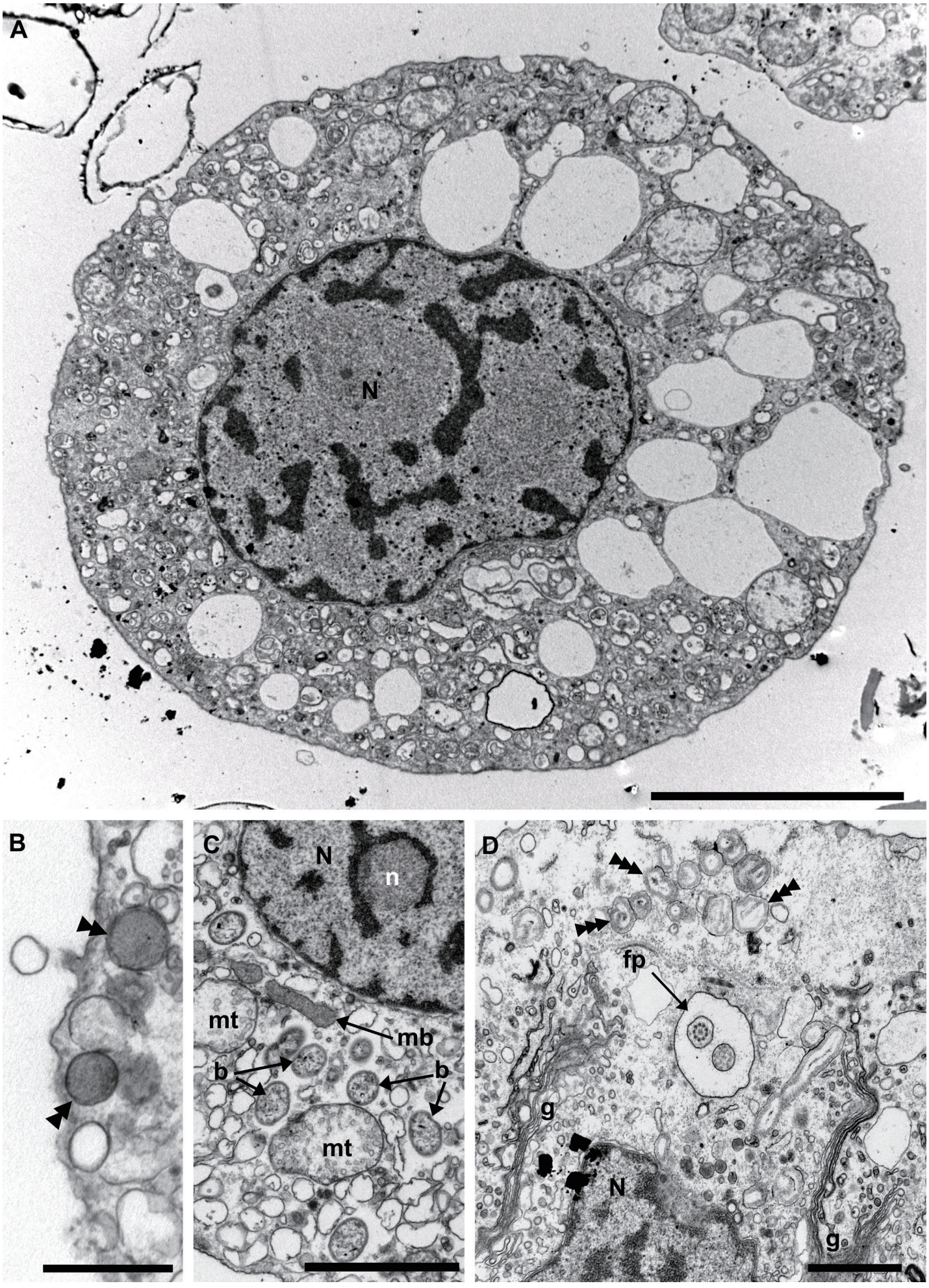

Fig. 5

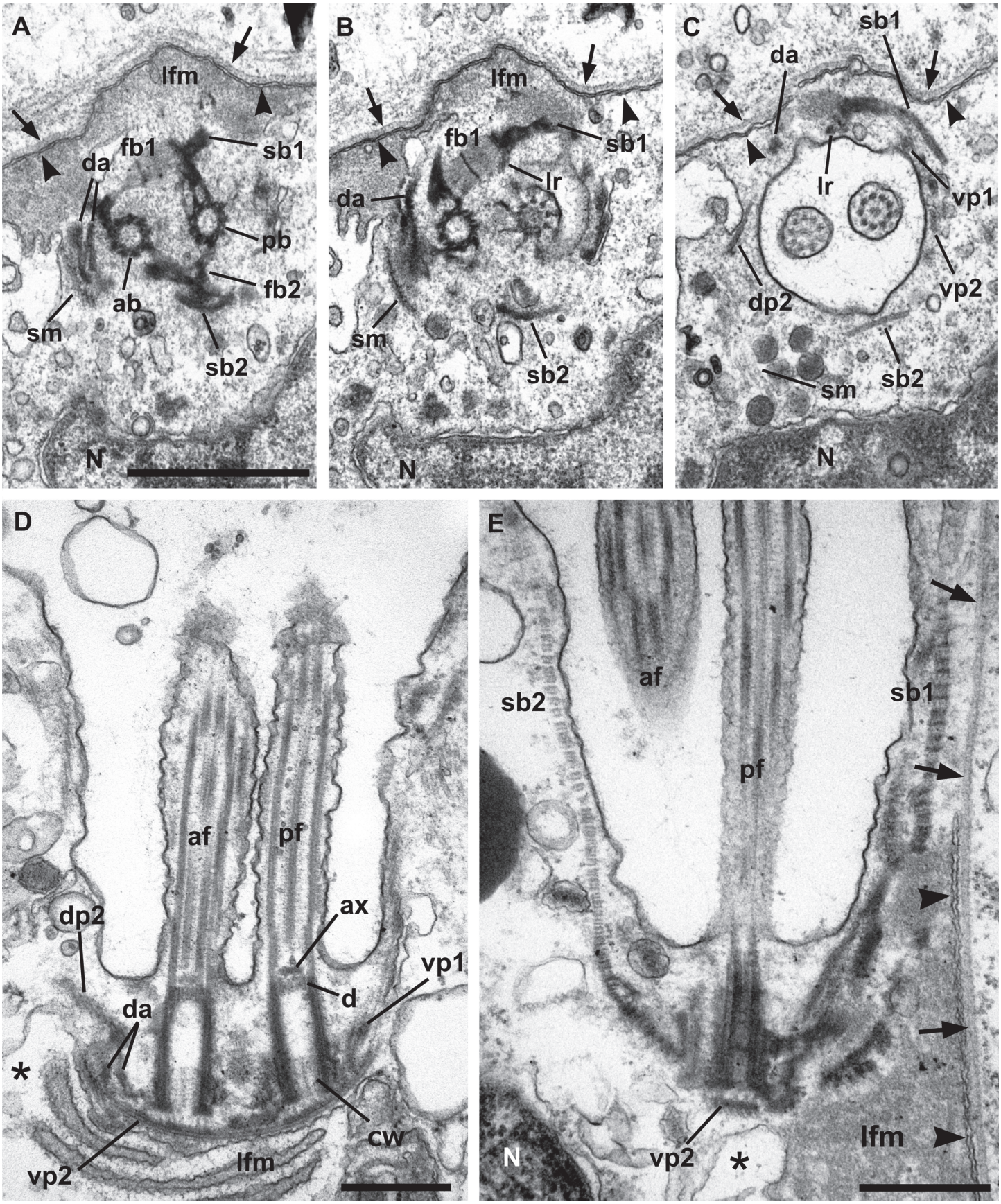
A
lfm
fb1
sb1
da
pb
fb2
ab
sm
sb2
N
B
lfm
fb1
sb1
lr
da
sm
sb2
N
C
sb1
da
lr
vp1
dp2
vp2
sm
sb2
N
D
af
pf
ax
dp2
vp1
d
da
*
cw
vp2
lfm
E
af
sb2
sb1
pf
N
vp2
*
lfm

Fig. 6

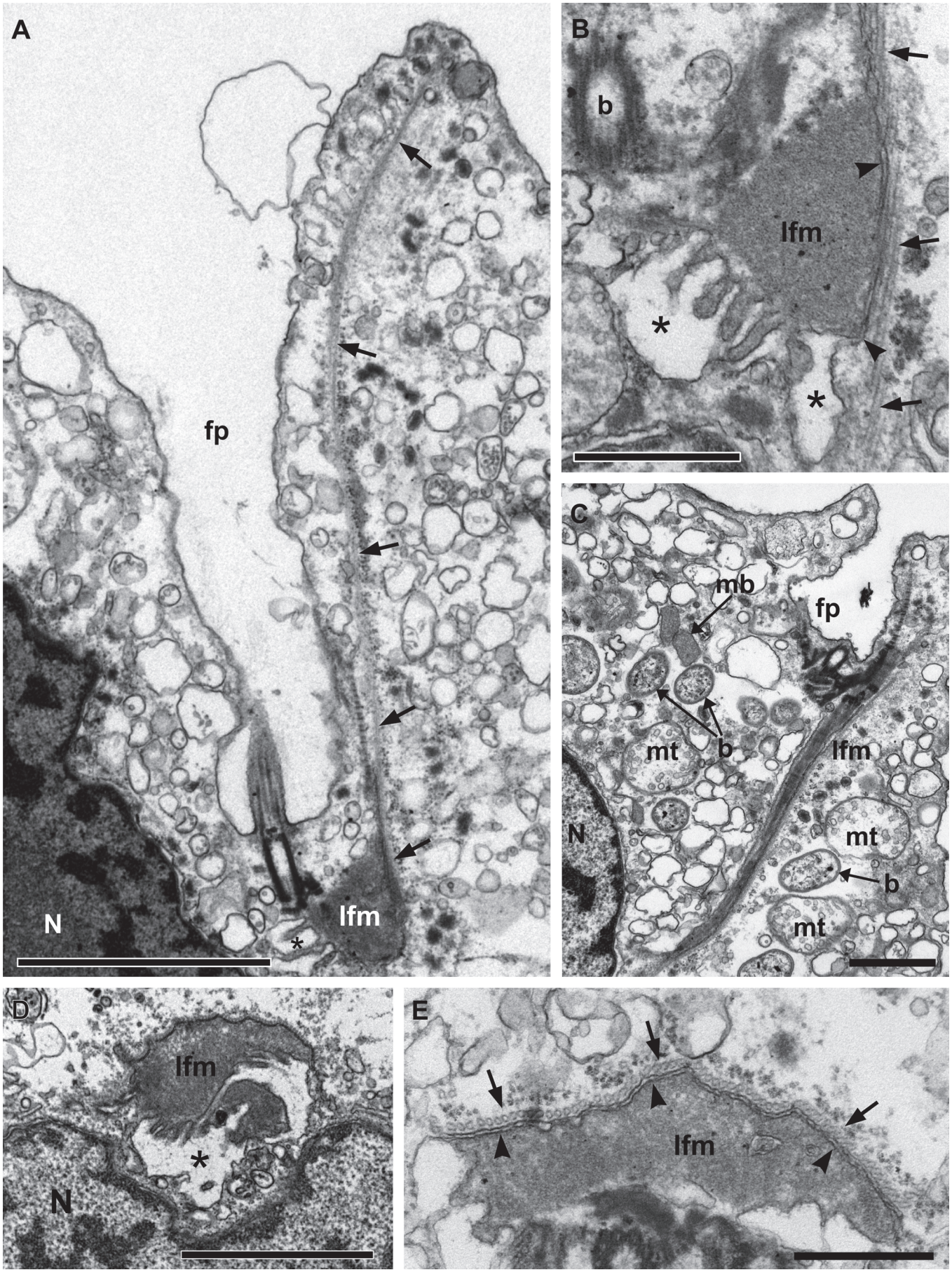

Fig. 7

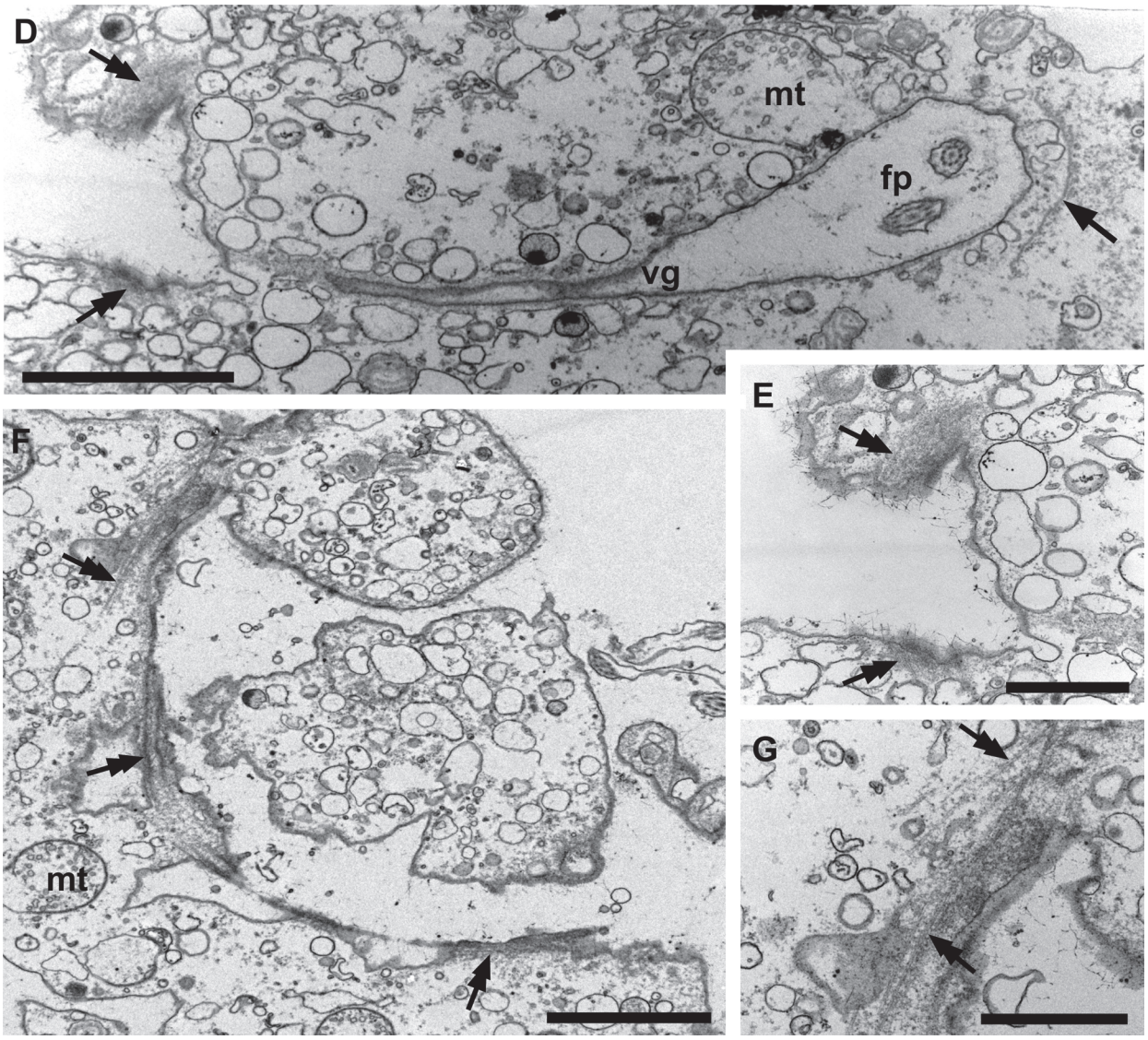

Fig. 8

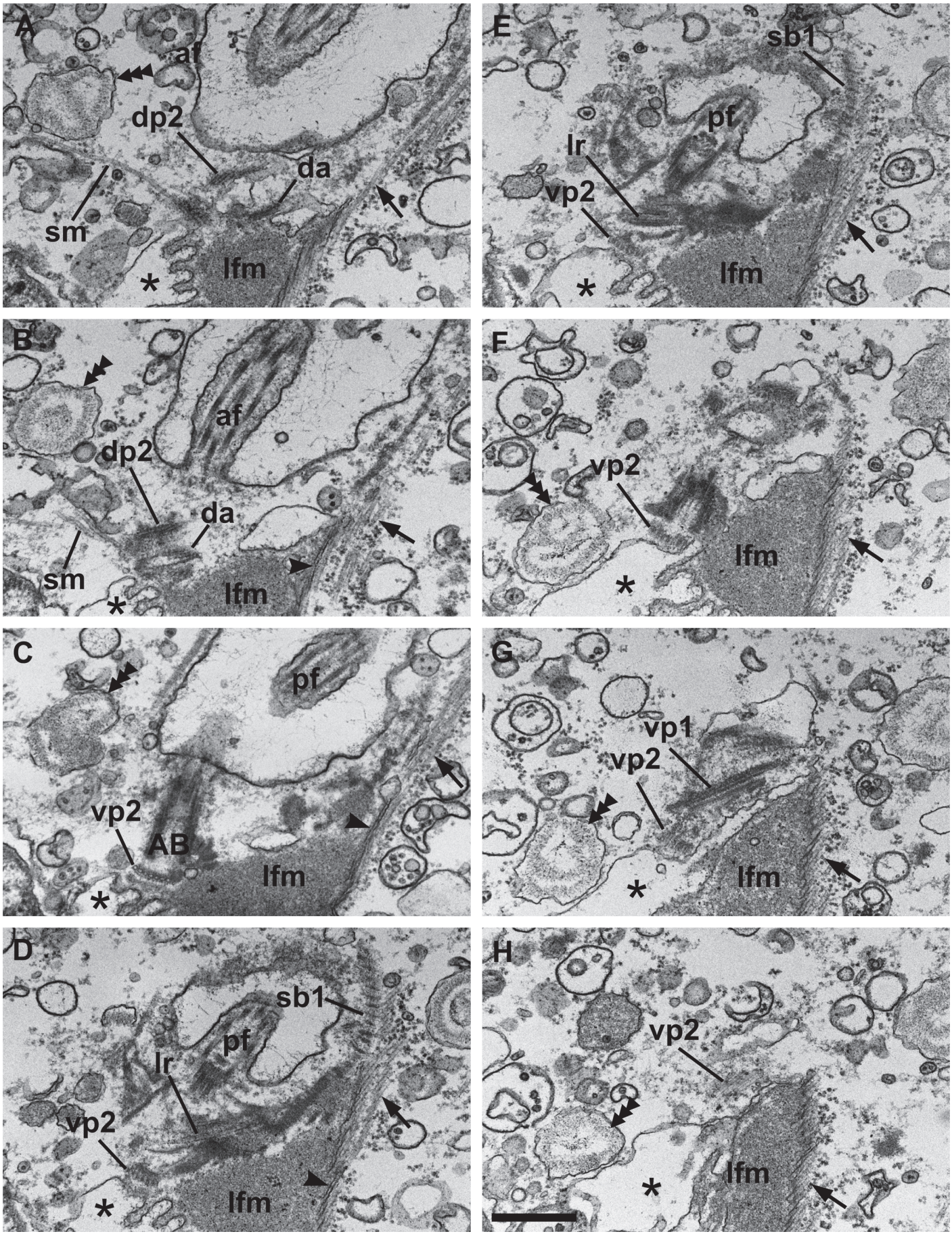
A
af
dp2
da
sm
lfm
*
E
sb1
pf
lr
vp2
lfm
*
B
af
dp2
da
sm
lfm
*
F
vp2
lfm
*
C
pf
vp2
AB
lfm
*
G
vp1
vp2
lfm
*
D
sb1
pf
lr
vp2
lfm
*
H
vp2
lfm
*

Fig. 9

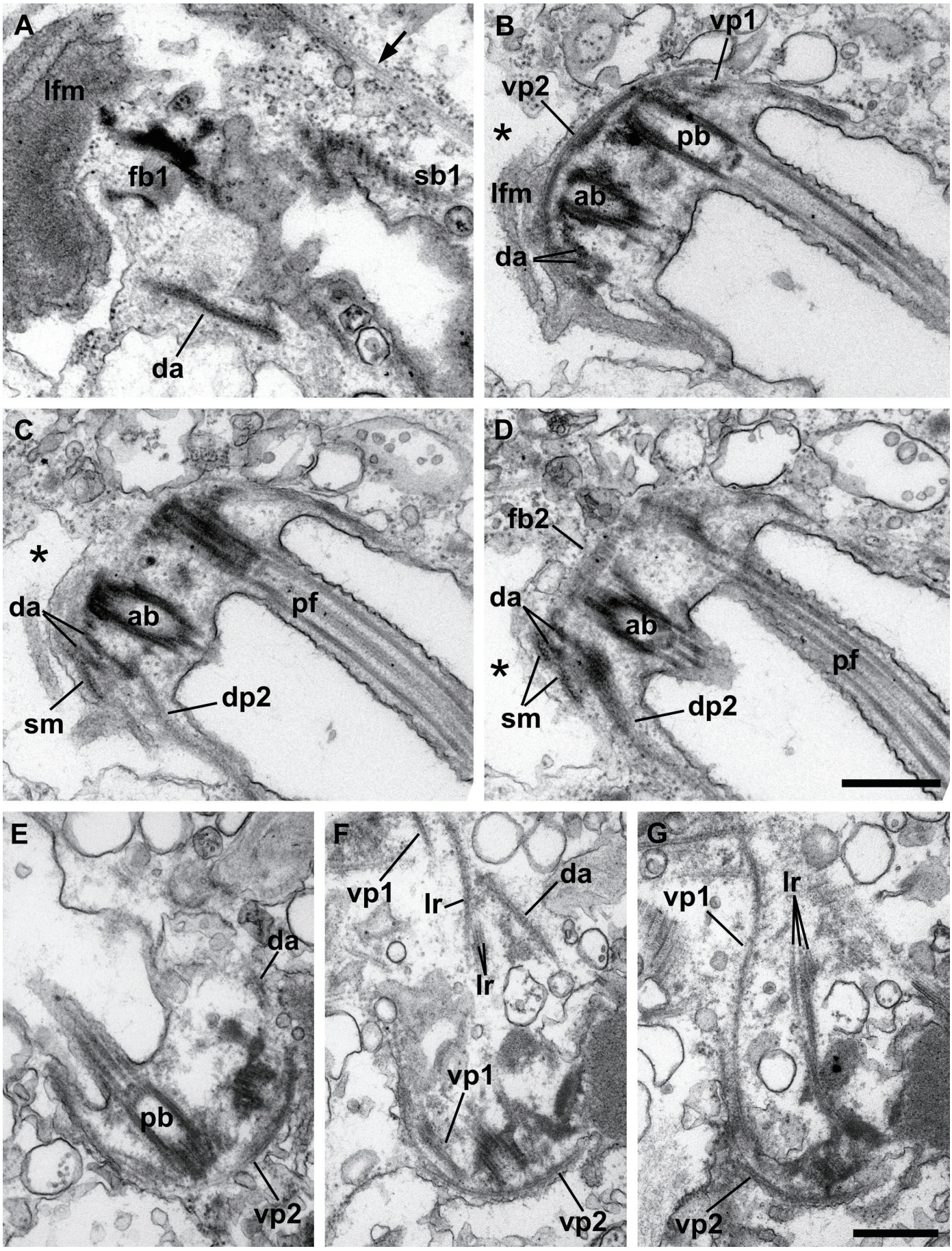
A
lfm
fb1
sb1
da
B
vp1
vp2
*
pb
lfm
ab
da
C
*
da
ab
pf
sm
dp2
D
fb2
da
ab
*
pf
sm
dp2
E
da
pb
vp2
F
vp1
lr
da
lr
vp1
vp2
G
vp1
lr
vp2

Fig. 10

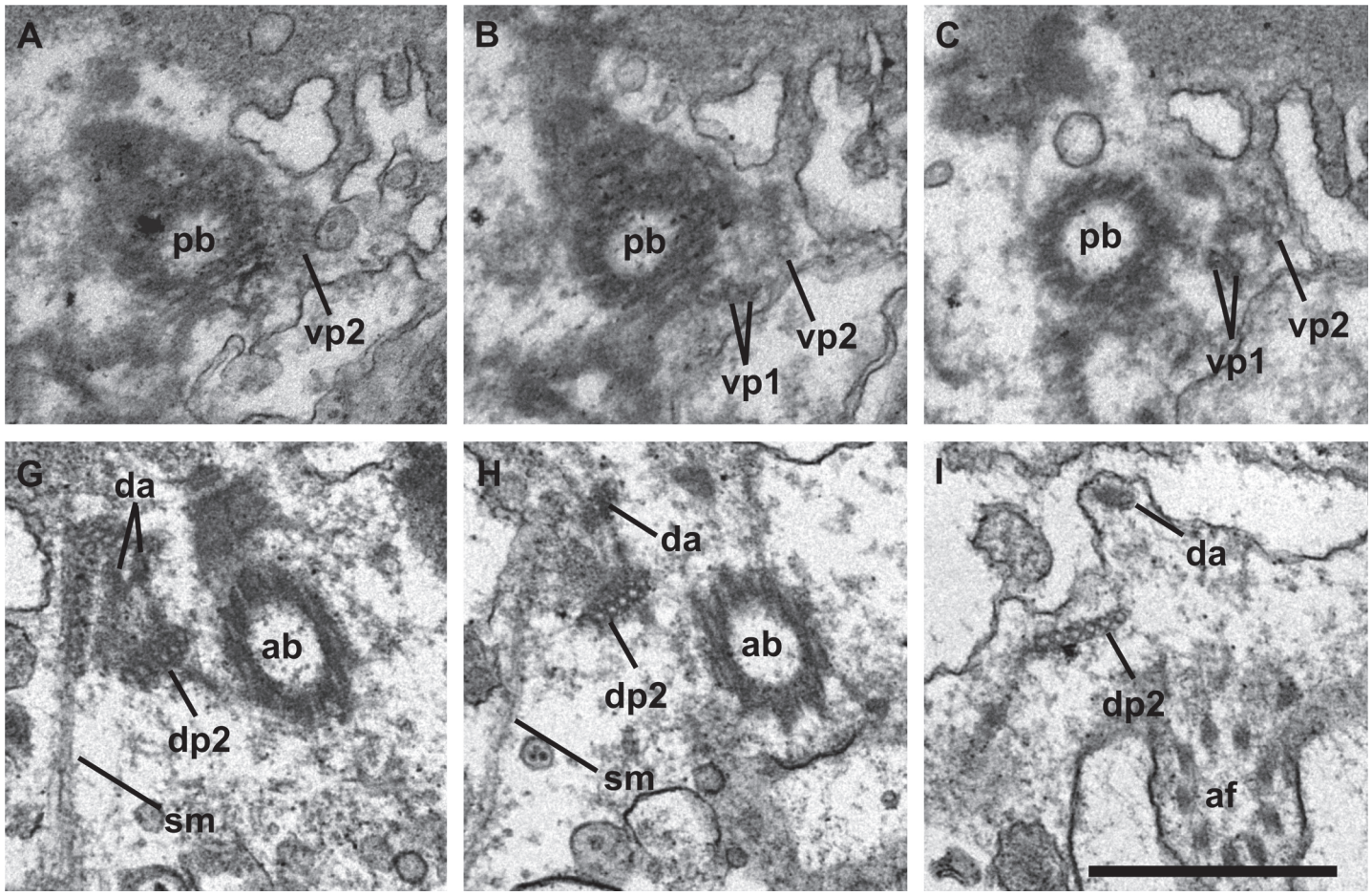
A
pb
vp2
B
pb
vp2
vp1
C
pb
vp1
vp2
G
da
ab
dp2
sm
H
da
ab
dp2
sm
I
da
dp2
af

Fig. 11

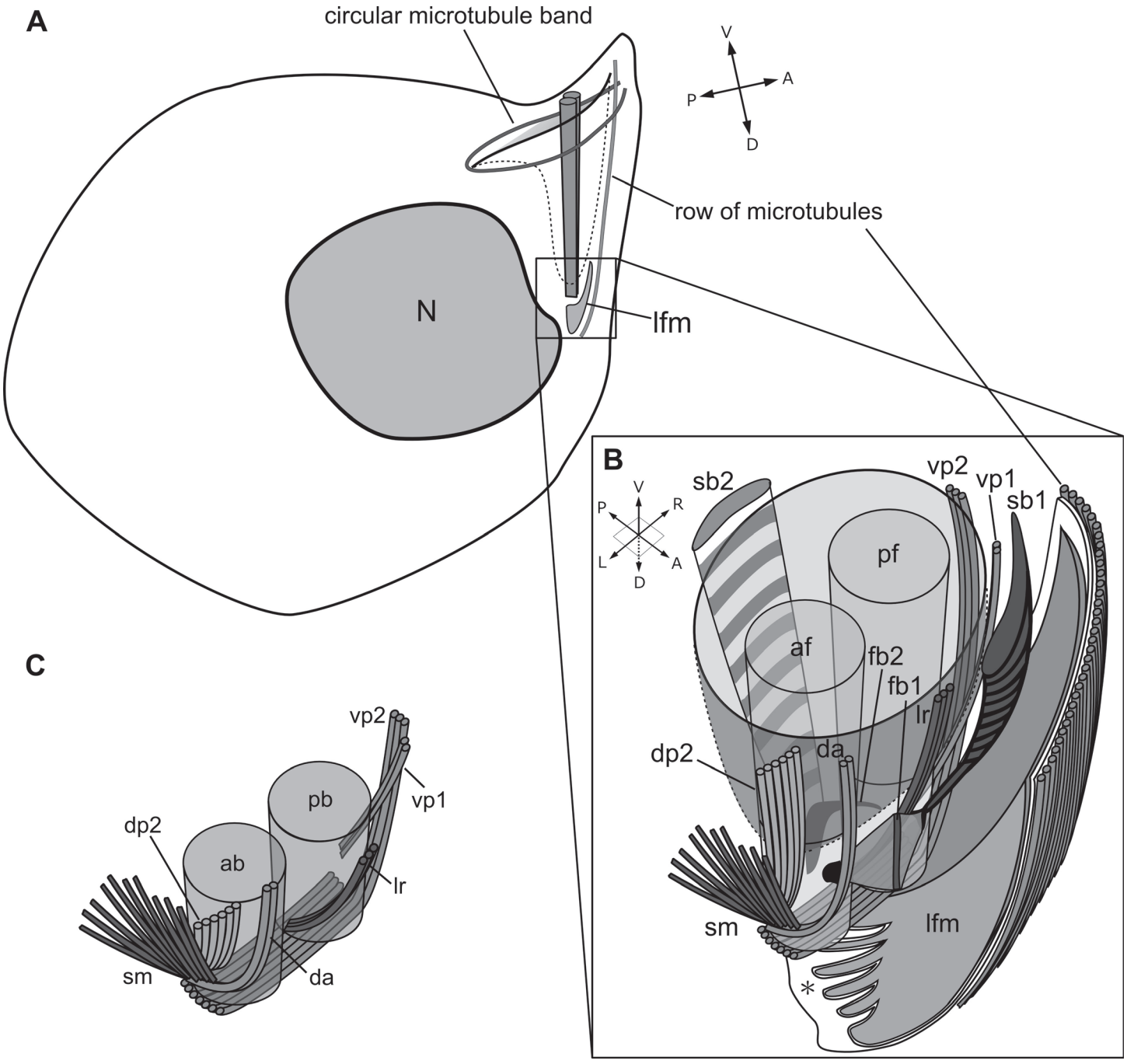
A
circular microtubule band
V
A
P
D
row of microtubules
N
lfm
B
V
P
R
L
A
D
sb2
vp2
vp1
sb1
pf
af
fb2
fb1
lr
dp2
da
sm
lfm
*
C
vp2
vp1
pb
dp2
ab
lr
sm
da

Fig. 12

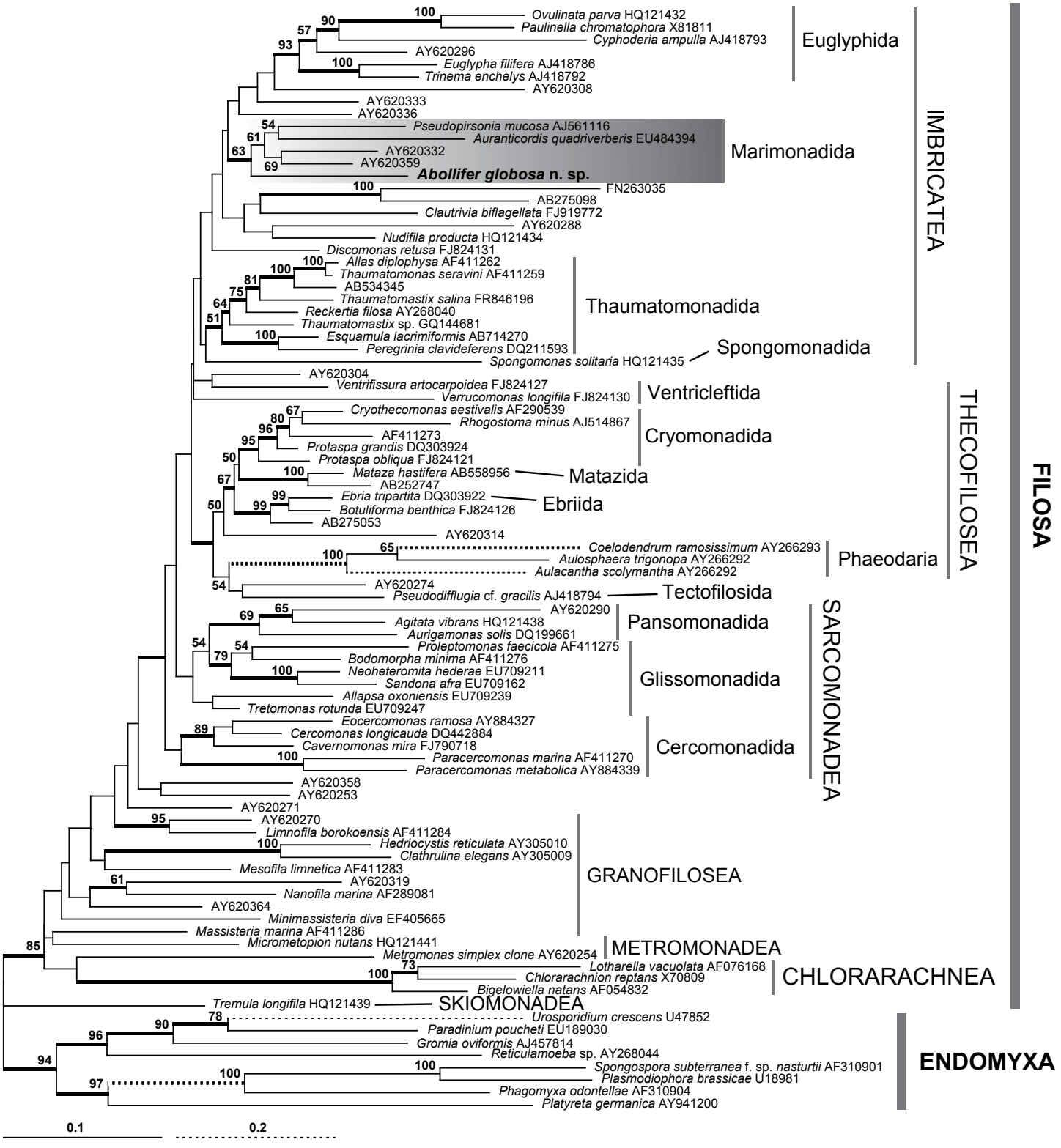
Ovulinata parva HQ121432
Paulinella chromatophora X81811
Cyphoderia ampulla AJ418793
AY620296
Euglypha filifera AJ418786
Trinema enchelys AJ418792
AY620308
AY620333
AY620336
Euglyphida
Pseudopirsonia mucosa AJ561116
Auranticordis quadriverberis EU484394
AY620332
AY620359
Abollifer globosa n. sp.
Marimonadida
FN263035
AB275098
Clautrivia biflagellata FJ919772
AY620288
Nudifila producta HQ121434
Discomonas retusa FJ824131
Allas diplophysa AF411262
Thaumatomonas seravini AF411259
AB534345
Thaumatomastix salina FR846196
Reckertia filosa AY268040
Thaumatomastix sp. GQ144681
Esquamula lacrimiformis AB714270
Peregrinia clavideferens DQ211593
Thaumatomonadida
Spongomonas solitaria HQ121435
Spongomonadida
IMBRICATEA
AY620304
Ventrifissura artocarpoidea FJ824127
Verrucomonas longifila FJ824130
Ventricleftida
Cryothecomonas aestivalis AF290539
Rhogostoma minus AJ514867
AF411273
Protaspa grandis DQ303924
Protaspa obliqua FJ824121
Cryomonadida
Mataza hastifera AB558956
AB252747
Matazida
Ebria tripartita DQ303922
Botuliforma benthica FJ824126
AB275053
Ebriida
AY620314
Coelodendrum ramosissimum AY266293
Aulosphaera trigonopa AY266292
Aulacantha scolymantha AY266292
Phaeodaria
AY620274
Pseudodifflugia cf. gracilis AJ418794
Tectofilosida
THECOFILOSEA
AY620290
Agitata vibrans HQ121438
Aurigamonas solis DQ199661
Pansomonadida
Proleptomonas faecicola AF411275
Bodomorpha minima AF411276
Neoheteromita hederae EU709211
Sandona afra EU709162
Allapsa oxoniensis EU709239
Tretomonas rotunda EU709247
Glissomonadida
Eocercomonas ramosa AY884327
Cercomonas longicauda DQ442884
Cavernomonas mira FJ790718
Paracercomonas marina AF411270
Paracercomonas metabolica AY884339
Cercomonadida
SARCOMONADEA
AY620358
AY620253
AY620271
AY620270
Limnofila borokoensis AF411284
Hedriocystis reticulata AY305010
Clathrulina elegans AY305009
Mesofila limnetica AF411283
AY620319
Nanofila marina AF289081
AY620364
Minimassisteria diva EF405665
Massisteria marina AF411286
Micrometopion nutans HQ121441
GRANOFILOSEA
Metromonas simplex clone AY620254
METROMONADEA
Lotharella vacuolata AF076168
Chlorarachnion reptans X70809
Bigelowiella natans AF054832
CHLORARACHNEA
Tremula longifila HQ121439
SKIOMONADEA
Urosporidium crescens U47852
Paradinium poucheti EU189030
Gromia oviformis AJ457814
Reticulamoeba sp. AY268044
Spongospora subterranea f. sp. nasturtii AF310901
Plasmodiophora brassicae U18981
Phagomyxa odontellae AF310904
Platyreta germanica AY941200
ENDOMYXA
FILOSA
0.1
0.2